# Atomic Layer Deposition of ZnO on InP Quantum Dot Films for Charge Separation, Stabilization, and Solar Cell Formation

Crisp, Ryan W.; Hashemi, Fatemeh S.M.; Alkemade, Jordi; Kirkwood, Nicholas; Grimaldi, Gianluca; Kinge, Sachin; Siebbeles, Laurens D.A.; van Ommen, J. Ruud; Houtepen, Arjan J.

**DOI**
10.1002/admi.201901600

**Publication date**
2020

**Document Version**
Final published version

**Published in**
Advanced Materials Interfaces

ADVANCED MATERIALS INTERFACES
www.advmatinterfaces.de



# Atomic Layer Deposition of ZnO on InP Quantum Dot Films for Charge Separation, Stabilization, and Solar Cell Formation

*Ryan W. Crisp,* Fatemeh S. M. Hashemi, Jordi Alkemade, Nicholas Kirkwood, Gianluca Grimaldi, Sachin Kinge, Laurens D. A. Siebbeles, J. Ruud van Ommen, and Arjan J. Houtepen**

**To improve the stability and carrier mobility of quantum dot (QD) optoelectronic devices, encapsulation or pore infilling processes are advantageous. Atomic layer deposition (ALD) is an ideal technique to infill and overcoat QD films, as it provides excellent control over film growth at the sub-nanometer scale and results in conformal coatings with mild processing conditions. Different thicknesses of crystalline ZnO films deposited on InP QD films are studied with spectrophotometry and time-resolved microwave conductivity measurements. High carrier mobilities of 4 $cm^2$ $(V\ s)^{-1}$ and charge separation between the QDs and ZnO are observed. Furthermore, the results confirm that the stability of QD thin films is strongly improved when the inorganic ALD coating is applied. Finally, proof-of-concept photovoltaic devices of InP QD films are demonstrated with an ALD-grown ZnO electron extraction layer.**

## 1. Introduction

Colloidal semiconductor quantum dot (QD) thin films have various applications in optoelectronic devices because of an easily adjustable bandgap, solution-based processing, and the potential to overcome the Shockley–Queisser limit in solar cells by exploiting carrier multiplication.[1–7] Due to their high surface-to-volume ratio many QD materials suffer from oxidative and photothermal degradation; this is detrimental to the material properties.[8–11] One way of improving the stability is synthesizing core–shell structures, but this often prevents extraction of one or both charge carriers.[12–15]

An alternative method that circumvents this problem is to encapsulate QDs after film formation when they are already electronically coupled. Ideally, the infilling material could provide both increased stability and enhanced charge separation, as is the case in bulk heterojunction solar cells. If a QD film is infilled with a semiconductor material that is characterized by a type II band offset with the QDs, as shown schematically in **Figure 1**, then the resulting heterostructure can induce a separation between the two carriers (electrons and holes) while improving the film stability by blocking the diffusion of ambient oxidants to the QDs. If the band offsets are engineered to the correct energy levels it could also be possible to use this band alignment engineering scheme to enhance carrier multiplication (CM)—a process that creates multiple free electrons from one high-energy photon.[16–21] It was recently shown that the use of heterojunctions provides a systematic way to reduce the threshold energy for CM.[22–24] Here we seek to form type II infilled QD films and focus on charge separation and transport in these heterojunctions.

The encapsulation process should provide protection against oxidation without hindering the electron transport properties or causing sintering of the QDs. Thus, a low-temperature coating process with the ability to uniformly and conformally cover the QDs would be of interest. A natural choice to accomplish those goals is atomic layer deposition (ALD).[25–27] ALD is a technique that allows for monolayer thickness control and uniformly coated surfaces as the molecular species react and attach to the surface and not to each other, thus limiting the growth. This surface-limited reaction can be used to coat materials with high aspect ratios and penetrate into void spaces of porous materials.[28–32]

Metal oxide deposition via ALD can be achieved within a wide range of temperatures, allowing to infill a QD film while avoiding QD sintering. One drawback of ALD is that it

Dr. R. W. Crisp,[+] Dr. F. S. M. Hashemi, J. Alkemade, Dr. N. Kirkwood,[++] Dr. G. Grimaldi, Prof. L. D. A. Siebbeles, Prof. J. R. van Ommen, Dr. A. J. Houtepen
Department of Chemical Engineering
Delft University of Technology
2629HZ, Delft, The Netherlands
E-mail: Ryan.Crisp@fau.de; A.J.Houtepen@TUDelft.nl
Dr. S. Kinge
Toyota Motor Europe
Materials Research & Development
1930 Zaventem, Belgium
The ORCID identification number(s) for the author(s) of this article can be found under https://doi.org/10.1002/admi.201901600.



[+]Present address: Department of Chemistry and Pharmacy, Friedrich-Alexander University Erlangen-Nuremberg, 91058 Erlangen, Germany
[++]Present address: ARC Centre of Excellence in Exciton Science, School of Chemistry, The University of Melbourne, Melbourne, Victoria, Australia

**DOI: 10.1002/admi.201901600**

 

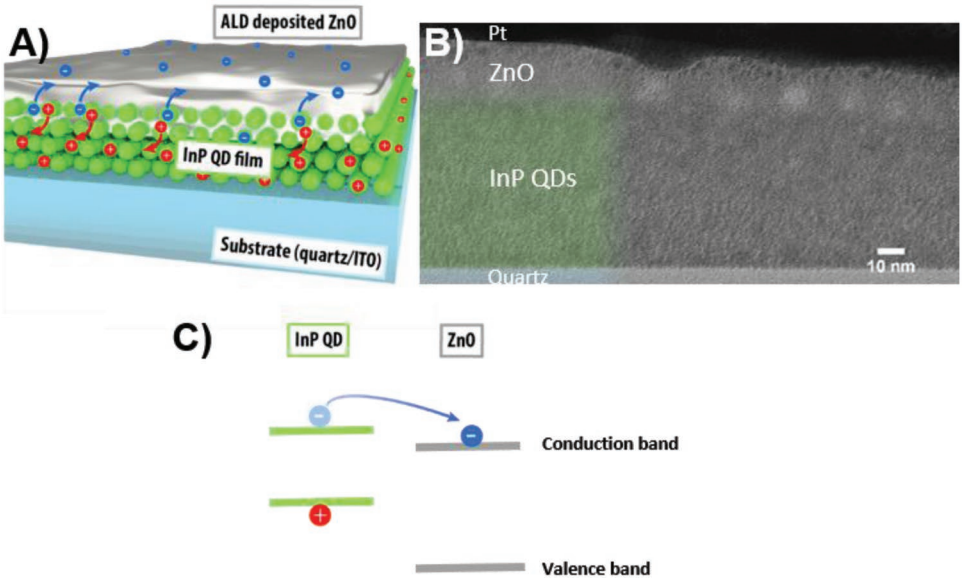


**Figure 1.** A) Schematic of an InP QD film infilled with ZnO to form a type II heterojunction. B) Cross-sectional TEM image showing over-coated InP QDs—false color is only on the leftmost portion of the image. C) Proposed type II heterojunction band level alignment.

is commonly a vacuum-based deposition technique, adding expense, and exposure to vacuum might negatively affect the properties of certain QD films due to evaporation of surface species.[33] However, we have developed an ambient-pressure ALD (AP-ALD) that uses only flowing $N_2$ to purge the chamber.[34] The benefits of this technique include scalability and process ease and it broadens the scope of materials that can be coated.[35,36]

Previous studies on ALD coating of QD films have looked at $Al_2O_3$ or ZnO growth on PbS(e) and CdSe QDs,[25–27,37–41] and have mostly focused on enhancing their (air) stability, rather than on making a functional coating that results in charge separation. Here we grow a functional electron transport layer of either $TiO_2$ or ZnO via ALD on Pb- and Cd-free InP QDs. The envisioned functions of these ALD coatings are to (1) cause charge separation, (2) reduce recombination, (3) enhance charge transport in the film, and (4) increase stability. After deposition and physical characterization of ZnO and $TiO_2$ on films of InP QDs, we measure with flash photolysis time-resolved microwave conductivity (TRMC) the resulting bicomponent films to investigate the charge carrier mobility and lifetime.[42–48] We demonstrate that the addition of ZnO coatings results in charge separation and a concomitant strong increase in photoconductivity and carrier lifetime. Motivated by these promising results, we demonstrate various QD solar cells of either InP QDs, PbS QDs, or CdTe QDs that makes use of an ALD-grown ZnO electron extraction layer.

## 2. Results and Discussion

Characterization of the ZnO film thickness versus the number of ALD cycles deposited on Si substrates using diethyl zinc (DEZ) and $H_2O$ in AP-ALD is shown in **Figure 2**a. The film thickness was monitored with ellipsometry. The observed growth rate of 2.8 ± 0.1 Å per cycle is in the range of reported literature values of 0.8–3.0 Å per cycle for various parameters.[49,50]

The absorption spectra of three thicknesses of ZnO films are plotted in Figure 2b and show an onset of 375 nm (≈3.31 eV), in line with the expected bandgap of ZnO.[51,52] The X-Ray diffraction (XRD) pattern shown in Figure 2c shows the expected pattern for wurtzite ZnO, while the broad diffraction lines are indicative of polycrystalline ZnO films. Scherrer analysis indicated that the ZnO domain size is ≈8–17 nm, as summarized in **Table 1**. X-Ray photoelectron spectroscopy (XPS) measurements of the ZnO film reveal an atomic ratio of 1:1.04 for Zn:O.

We investigated the photoconductivity upon excitation at 250 nm with a 3 ns laser pulse of the ZnO films with TRMC measurements. Figure 2d shows the resulting yield-mobility product which is the number of free charge carriers generated per absorbed photon times the sum of the electron and hole mobility calculated from the photoconductivity per absorbed photon as described elsewhere.[53] We observe that the yield-mobility product increases with increasing ZnO layer thickness, likely associated to the formation of a more continuous film and availability of an increasing number of charge transport pathways with increasing film thickness. It is also evident from Figure 2d that the signal decreases with increasing fluence. This is attributed to higher order recombination of charge carriers, such as Auger recombination.[54] The lines are fits to the data (see refs. [44,55–57]) and are used to extract the low-fluence mobility when higher order recombination is negligible. For the film thicknesses explored here, the mobility is 0.1–0.8 $cm^2$ $(V\ s)^{-1}$ if we assume that the yield of free charges is 1, where higher mobility correlates to thicker films. Such mobilities are sufficient for many optoelectronic applications.[58–60]

$TiO_2$ films produced at growth temperatures suitable for preserving the QD properties are amorphous.[61] The absorption spectrum and photoconductance of a 27 nm (99 cycles) thick film are shown in Figure S1 in the Supporting Information. The absorption onset around 350 nm is in line with the

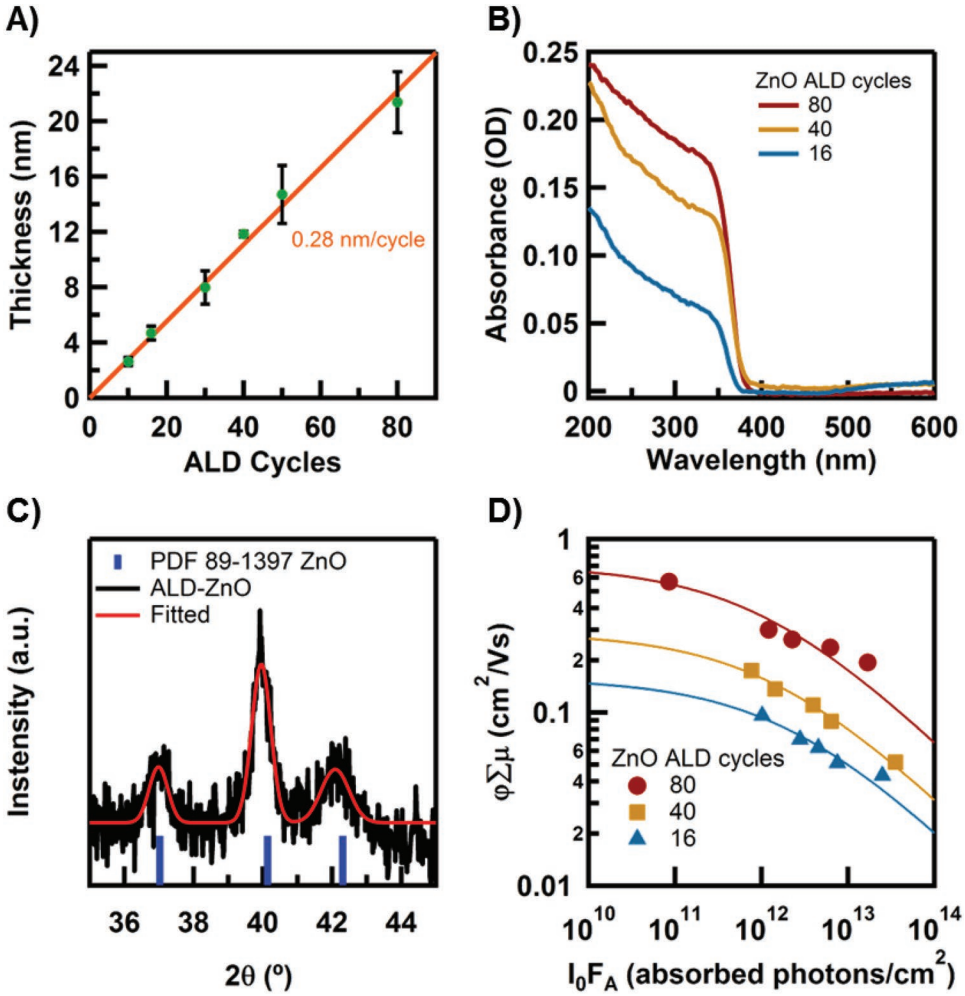


**Figure 2.** A) Film thickness of ZnO at different cycles measured with spectroscopic ellipsometry. The red line is a linear fit through the origin where the slope is the growth rate of the ALD process. The growth of this process is 2.8 ± 0.1 Å per cycle. B) Absorption spectra of ZnO films with an absorption onset around 3.3 eV. C) X-Ray diffraction pattern of 24 nm thick ZnO film on Si substrate showing the expected reflections (blue bars) and fitted (red line) to determine the crystal domain size. D) Time-resolved microwave conductivity measurements showing the yield times the sum of the electron and hole mobility versus the absorbed photon fluence. The mobility increases with increasing film thickness and lower fluence.

expected bandgap; however, the photoconductance is at the lower limit of the measurement, corresponding to a mobility of $2 \times 10^{-4}$ cm$^2$ (V s)$^{-1}$, hence more focus is placed on ZnO due to its superior optoelectronic properties, when grown with AP-ALD.

Next, we used ambient pressure ALD to deposit ZnO on films of InP QDs capped with $(NH_4)_2S$ ligands. We first investigate the elemental composition of the composite films using XPS depth-profiling. **Figure 3**a shows the atomic percentage of the main elements present in the films as a function of the etching time. Initially there is a strong Zn signal rapidly decreasing in intensity as the In signal increases. Figure 3 also shows the binding energy region for Zn 2p3 (panel B) and In 3d (panel C) XPS signals as a function of the etching time. It is clear that an overgrown layer of ZnO is present on top of the InP QD, and that Zn is present throughout the entire film, showing that infilling of ZnO took place. Cross-sectional transmission electron microscopy confirms a QD layer and overcoating ZnO layer (Figure 1b; Figure S2, Supporting Information). The amount of zinc inside the QD film is however small, with a near constant In:Zn atomic ratio of 5.4 and a higher than expected amount of oxygen perhaps due to partial oxidation of the InP during the ALD process.

**Table 1.** Crystal domain sizes for ZnO grown using AP-ALD calculated using the Scherrer equation.

| Crystal Plane | ZnO reference 2θ [°] | ZnO AP-ALD 2θ [°] | Domain size [nm] |
|---|---|---|---|
| 100 | 37.02 | 36.98 | 14.5 |
| 002 | 40.14 | 39.95 | 16.6 |
| 101 | 42.31 | 42.11 | 7.8 |

To determine the extent of infilling, let us approximate the InP QD film by close-packed spheres. The volume fraction of filled space is then $f_{InP} = 0.7405$. If we assume complete infilling with ZnO (i.e., $f_{ZnO} = 1 - f_{InP}$) we can deduce that the In:Zn ratio should be the ratio of the respective volumes divided by the volume per Zn or In atom in

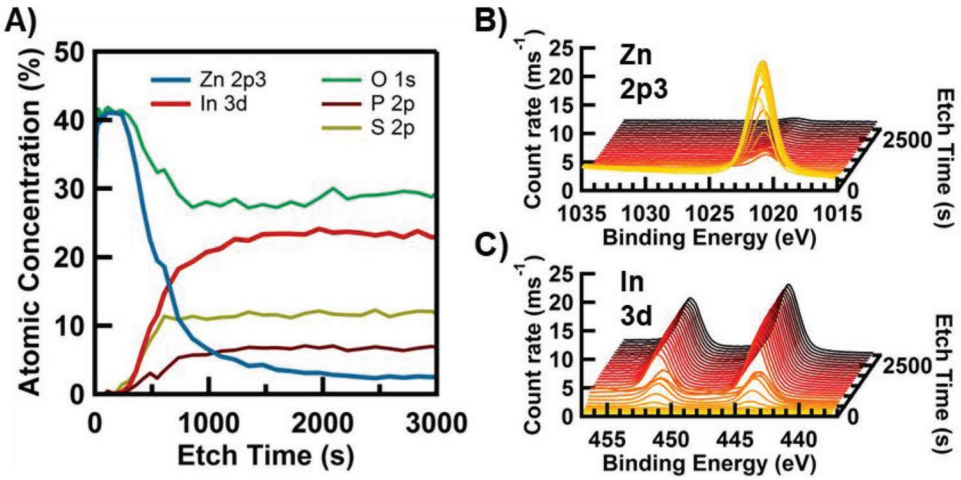


**Figure 3.** Depth-profiling of InP QDs coated with 30 nm of ZnO using X-Ray photoelectron spectra showing A) the atomic percentage of the main elements in the film as a function of etching time and photoelectron count rate in the binding energy range of B) Zn 2p3 and C) In 3d, indicating a clear spatial segregation of the ZnO and InP with slight in-filling of the voids between QDs.

ZnO and InP respectively, obtained as the unit cell volume divided by the number of Zn or In atoms per unit cell:[62,63]

$$\mathrm{In:Zn} = \frac{f_{\mathrm{InP}} * \#\,\mathrm{atoms} / V_{\mathrm{InP}}}{(1 - f_{\mathrm{InP}}) * \#\,\mathrm{atoms} / V_{\mathrm{ZnO}}} = \frac{0.7405 * 4/202.1}{0.2595 * 6/143.0} = 1.34.$$

See Note S1 in the Supporting Information for more details on this calculation.[62,63] If the void space were larger (as it most likely is for random close-packed QDs with short sulfide ligands),[62,64] then the In:Zn ratio would be smaller. The experimental ratio of 5.4 thus shows that infilling does occur but that it is quite incomplete.

**Figure 4**a shows the absorption spectrum of the starting QD film (gray trace) and the spectra of QD films after deposition of various amounts of ZnO. There is minimal bathochromic shift of the first exciton peak indicating little change in the characteristic size or composition of the QDs upon ZnO deposition. The resulting spectra do exhibit some increased absorption at shorter wavelengths, possibly caused by a reduction in the reflectivity of the film where the ZnO acts as an antireflection coating.

In Figure 4b, we compare the yield-mobility values of the ALD-coated films for different ZnO deposition cycles with the ZnO layer thicknesses measured using spectroscopic ellipsometry on planar Si witness substrates. The initial growth rate of ZnO on the InP QDs could be different than that of the Si witness and thus we report only the number of ALD cycles for the QD + ZnO films. The ZnO-only films were excited at 250 nm, while the InP QD containing films were excited at 500 nm to prevent direct excitation of the ZnO. Exciting the ZnO at 500 nm leads to ≈4 orders of magnitude lower signal (see Figure S3 in the Supporting Information), indicating no significant sub-gap absorption takes place. The ZnO-only films are shown as blue circles and have mobility values well above that of the InP-only QD film (the red triangle at 0 nm ZnO thickness). When ZnO is deposited on the InP QDs the mobility increases and surpasses that of the ZnO-only film for the thickest layers investigated here (24–30 nm), indicating a synergistic effect of incorporating ZnO into the films. Because the films are heated at 125 °C during the deposition the increase in mobility could result from fusing of the QDs. Even though the absorption spectra indicate negligible particle growth, a control experiment was performed by annealing the InP QD films at 125 °C and measuring the yield-mobility product which unexpectedly decreased (* symbol in Figure 4b). This shows that the increase in yield-mobility product for ALD coated InP QD films does not arise from QD sintering and can be attributed to the presence of ZnO in the films.

To investigate this increased photoconductivity, we show in Figure 4c photoconductivity transients for the films, normalized at their early-time maximum around 12–17 ns (which is approximately the instrumental response time). The InP-only film and the ZnO-only films show the same order of magnitude half-life times: ≈40 ns (InP) to ≈70 ns (ZnO). Coating the InP QDs with 16 ALD cycles (corresponding to 5.6 nm of ZnO on a witness planar substrate) results in more than double the yield-mobility product for the composite film but with a half-life time similar to the individual component films (65 ns).

Increasing the deposition of ZnO further, we see a drastic change in the kinetics. The transient signal has an initial increase that we attribute to the mobility of carriers within the InP QD layer. There is then a second increase in signal as electrons transfer to the over-coated ZnO film and become more mobile. Furthermore, this charge separation between the InP QD and ZnO leads to longer carrier lifetimes (in the range of tens of microseconds, Figure S4, Supporting Information) due to the reduced recombination of spatially separated carriers. This causes the yield-mobility product of the ALD-ZnO coated films to be even larger than of similarly thick ZnO only films.

These results show that ALD coating of InP QD films with ZnO indeed results in a functional type II heterojunction, with associated charge separation and enhanced carrier lifetimes. As a side benefit, the ZnO coating helps prevent the degradation of the InP QDs. InP QD exposed to air rapidly oxidize as indicated by a blue-shifting absorption spectrum and loss of absorption strength (i.e., the film becomes more transparent), while the ZnO coated film retains its optical properties (shown in Figure S5 in the Supporting Information).

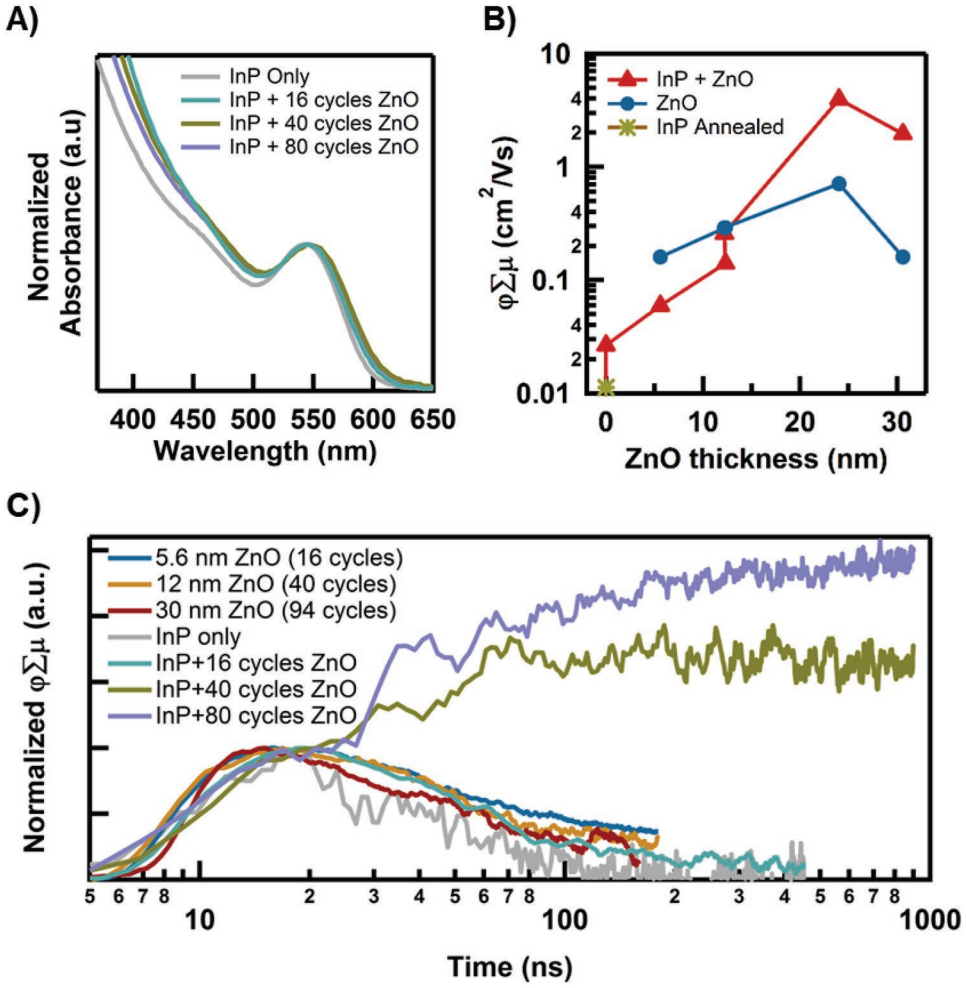


**Figure 4.** A) Absorption spectra of InP QD films normalized at the 1S peak with 5.6, 12, and 24 nm of ZnO deposition as measured on witness substrates. The minimal peak shifting and broadening indicate the QDs retain their quantum confinement. B) The peak of the yield-mobility product measured with TRMC for ZnO-only films directly photoexcited at 250 nm and InP QDs coated with various thicknesses of ZnO excited at 500 nm. The * symbol indicates the yield-mobility product of InP QD films annealed/treated in the same manner as the films coated with ZnO to control for heating effects. Lines are guides to the eye. C) Time-dependence of the yield-mobility product normalized at the maximum or ≈17 ns (the instrument response-time) for films of ZnO and InP QDs with various ZnO thicknesses.

In contrast to the favorable electronic properties of ZnO ALD coated InP QD films, deposition of $TiO_2$ at 125 °C on InP QDs leads to only modest mobility improvements from 0.02 to 0.2 $cm^2$ $(V\ s)^{-1}$ (Figure S6, Supporting Information). While the same charge separation could occur as in ZnO coated films, the amorphous $TiO_2$ has a low mobility resulting in little enhancement of the carrier transport in composite films. If the deposition temperature were increased to yield more crystalline $TiO_2$ this could possibly result in a larger enhancement of the measured mobility.[61] However, the QDs have a greater risk of sintering or morphological changes with increased temperature.[40,65] Therefore, ZnO appears to be the material of choice for the formation of type II heterojunction via ALD infilling.

Charge separation between the InP and ZnO leads to the possibility of forming a rectifying junction for use in either LEDs or solar cells. To demonstrate the applicability of ALD infilling for such applications we have fabricated prototype solar cells with a device structure of glass/indium tin oxide (ITO)/poly(3,4-ethylenedioxythiophene) polystyrene sulfonate (PEDOT:PSS)/InP QDs/ALD-ZnO/Al. Current–voltage curves of such a device are shown in **Figure 5**a. This device shows clear photovoltaic action with a power conversion efficiency (PCE) of 0.41%. The device exhibits a low short-circuit current ($J_{sc}$) and reverse bias current leakage perhaps due to it being too thin: the presence of cracks in the InP QD films means that the ZnO/Al layers can contact the PEDOT:PSS and cause shunting. Applying the ALD-ZnO on devices of PbS QDs with the same structure yields a PCE of 0.77% (Figure 5b) mainly limited by the low open circuit voltage which is typical for this device structure.[1] Likewise, CdTe solar cells made similarly but without the PEDOT:PSS show an efficiency of 0.77% but are limited by the short-circuit current (Figure 5c). Although rigorous optimization is needed to achieve higher efficiencies, these concept devices show great potential for the integration of a functional ALD-grown metal-oxide layer to provide charge extraction in solar cell devices.

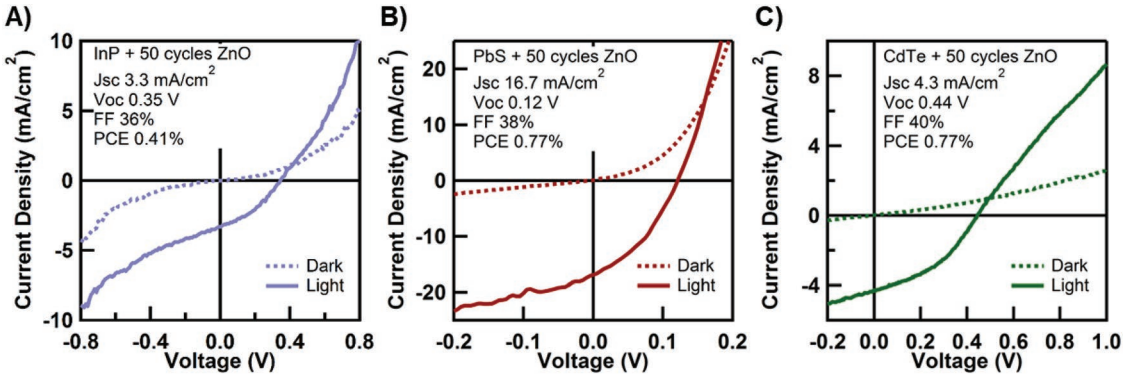


**Figure 5.** Current density versus voltage (*JV*) curves of ITO/PEDOT:PSS/QDs/ALD-ZnO/Al solar cell with 50 cycles of ALD ZnO. A) InP QDs, B) PbS QDs, and C) sintered CdTe QDs without the PEDOT:PSS layer.

## 3. Conclusions

Utilizing ambient-pressure ALD to infill and coat InP QD films leads to high mobility films with efficient charge separation that are an ideal platform for device applications. The ZnO deposited acts as an electron accepting layer improving the carrier mobility and lifetime by two and three orders of magnitude, respectively. The air-stability of composite films is drastically improved with no qualitative change in the optical absorption of films stored in ambient conditions. Utilizing AP-ALD ZnO in conjunction with InP QDs, PbS QDs, and sintered CdTe QDs for prototype solar cells demonstrates optoelectronic functionality with modest efficiencies from 0.4% to 0.8% PCE. With more optimization, perovskite, PbS, PbSe, and/or CdTe QD solar cells would all benefit from the improved charge carrier separation, higher carrier mobility, and encapsulation offered by the facile AP-ALD process presented here.[66–68]

## 4. Experimental Section

Chemicals were purchased from Sigma Aldrich at the highest purity available and used as received unless stated otherwise.

*InP QD Synthesis and Film Preparation*: QDs were synthesized following our previously reported procedure without incorporation of Zn.[69,70] The palmitate on the surface of the washed InP QDs was exchanged for $S^{2-}$ in solution as described elsewhere.[69,71] Briefly, 1 mL of InP QDs in hexane was pipetted on top of 1 mL of neat dimethylformamide (DMF). 100 µL of 1 M $(NH_4)_2S$ in formamide (FA) (prepared by adding aqueous $(NH_4)_2S$ 48% in water to FA, sparging under $N_2$ for 20 min, and adding 5 Å molecular sieves to dry before bringing into the glovebox). The solution was stirred until the QDs completely transferred to the bottom DMF phase. The QDs were rinsed three times with neat hexane by adding hexane, shaking the solution, and pipetting off the hexane. The QDs were then precipitated by adding acetonitrile and centrifugation at 1800 rcf before being dispersed in 0.5 mL of DMF. Films were drop-cast onto UV-ozone cleaned quartz substrates at 50 °C yielding thicknesses around 100 nm as measured with a Dektak profilometer.

*Atomic Layer Deposition*: The atmospheric pressure ALD experiments were carried out in a home-built reactor operating at atmospheric pressure as described elsewhere.[72] The AP-ALD chamber consists of a glass column (50 mm in internal diameter and 200 mm in height). The Zn precursor (DEZ) was contained in a stainless-steel bubbler and kept at room temperature. The stainless-steel tubing connecting the bubbler and the reactor was maintained at 80 °C. Water was used as the counter-reactant and was kept in a stainless-steel bubbler at room temperature. The reactor was heated at 125 °C by an infrared lamp placed parallel to the column with feedback control to maintain a constant temperature during AP-ALD. The precursor was carried to the reactor column with a nitrogen gas flow of 0.5 L $min^{-1}$. The process consisted of sequential exposures of the substrates to 2 s of Zn precursor and 2 s of water, separated by a nitrogen purging step of 5 min. This process resulted in a growth rate of 2.7 Å per cycle for ZnO films which was measured on a reference Si substrate with spectroscopic ellipsometry (J. A. Woollam M2000 D) at an incident angle of 75.68°. ZnO and $TiO_2$ film thicknesses were fitted using Gen-Oscillator and Cauchy models, respectively.

AP-ALD of $TiO_2$ was done using $TiCl_4$ as the reactant and water as the oxidizer, both were stored in stainless still bubblers at room temperature. The reactor temperature was kept at 125 °C. During each ALD cycle, 2 s pulses of $TiCl_4$ and water were applied separated by a purging step of 5 min.

*X-Ray Diffraction*: XRD was performed on a Bruker D8 Advance using a Co-K$\alpha$ source on samples prepared on glass or ITO/glass substrates.

*Transmission Electron Microscopy*: TEM cross-sections were made using a FEI Helios G4 CX to ion mill a lamella that was then imaged on a JEOL JEM3200-FSC operating at 300 kV with a Gatan K2-Summit camera in counting mode. Energy dispersive X-ray (EDX) analysis was performed on a JEOL-JEM1400 plus microscope operating at 120 kV.

*X-Ray Photoelectron Spectroscopy*: XPS was done on a Thermo Scientific K-Alpha system with a spot size of 400 µm and 1486.7 eV. Depth profiling was performed using $Ar^+$ beam. Peak fittings and depth profiling analyses were done using Thermo Avantage Software.

*Time-Resolved Microwave Conductivity*: TRMC is a contactless spectroscopic technique relating the change in microwave probe power to the sum of electron and hole mobility, $(\mu_e + \mu_h)$ multiplied by the yield of charge carrier generation, $\varphi(t)$, which is a function of time as the photoexcited charges recombine. TRMC measurements were performed in a microwave cavity and photoexcited with a 3 ns laser as described in detail elsewhere.[44,53,69]

*Solar Cell Fabrication*: Solar cells were fabricated on ITO-coated glass substrates purchased from Ossila and sonicated in ethanol, acetone, and DI water each for 5 min then UV-ozone treated and spin coated with PEDOT:PSS (Al 4083, purchased from Ossila) at 2000 rpm. The PEDOT:PSS was heated on a hotplate at 125 °C for 10 min. InP QDs solution-phase ligand exchanged with $(NH_4)_2S$ were drop-cast from DMF on the substrates and dried at 50 °C. Two layers of PbS QDs (fabricated as discussed in Refs. [67,73,74]), were spin-coated from octane at 2000 rpm and treated with $10 \times 10^{-3}$ M ethane dithiol (EDT) in acetonitrile for 10 s and rinsed with neat acetonitrile. Four more layers were deposited via spin coating and treating with $PbI_2$ in DMF and rinsed with acetonitrile. CdTe solar cells were made on ITO glass without the PEDOT:PSS (which would not withstand the annealing process)

using the recipe given in Refs. [75–77] Briefly, eight layers of CdTe QDs were spin coated at 1000 rpm with a $CdCl_2$ treatment and annealing on a hotplate at 350 °C for 10 s between each layer. After coating with ALD ZnO, 200 nm of Al was thermally evaporated at a rate of 1.5–2 Å $s^{-1}$. Devices were measured under simulated AM 1.5 conditions (OAI class AAA solar simulator) in a $N_2$-filled glovebox.

*Transient Absorption*: TA measurements were performed using a Yb:KGW oscillator (Light Conversion, Pharos SP) with the fundamental beam sent through an Optical Parametric Amplifier (OPA) with a second harmonic module (Light Conversion, Orpheus) to produce an output beam. Part of the fundamental beam is used to generate a broadband probe spectrum (450–1600 nm) through a sapphire crystal. Pump and probe beam overlap at an angle of ≈8° at the sample position, with the time delay controlled by an automated delay-stage. The differential absorbance is calculated via $\Delta A = \ln(I_{on}/I_{off})$, where $I$ is the light power incident on the detector with either pump-on or pump-off.

## Supporting Information

Supporting Information is available from the Wiley Online Library or from the author.

## Acknowledgements

R.W.C., G.G., L.D.A.S., and A.J.H. were supported by STW (project No. 13903, Stable and Non-Toxic Nanocrystal Solar Cells). A.J.H. further acknowledges support from the European Research Council Horizon 2020 ERC Grant Agreement No. 678004 (Doping on Demand). The authors thank Bart Boshuizen for assistance in acquiring the XPS data, Ben Norder for assistance in acquiring the XRD data, Hozanna Miro for preparing the TEM cross-section, and Wiel H. Evers for acquiring the TEM images.

## Conflict of Interest

The authors declare no conflict of interest.

## Keywords

charge transport, LEDs, p–n junctions, quantum dots, solar cells, time-resolved microwave conductivity

Received: September 19, 2019
Revised: December 11, 2019
Published online:

[1] A. A. Ganesan, A. J. Houtepen, R. W. Crisp, *Appl. Sci.* **2018**, *8*, 1867.
[2] T. Ghosh, A. Gopal, S. Nagasawa, N. Mohan, A. Saeki, V. C. Nair, *ACS Appl. Mater. Interfaces* **2016**, *8*, 25396.
[3] N. Kirkwood, J. O. V. Monchen, R. W. Crisp, G. Grimaldi, H. A. Bergstein, I. du Fossé, W. van der Stam, I. Infante, A. J. Houtepen, *J. Am. Chem. Soc.* **2018**, *140*, 15712.
[4] R. W. Crisp, G. Grimaldi, L. De Trizio, W. Evers, N. Kirkwood, S. Kinge, L. Manna, L. Siebbeles, A. J. Houtepen, *Nanoscale* **2018**, *10*, 11110.
[5] D. A. Wheeler, J. Z. Zhang, *Adv. Mater.* **2013**, *25*, 2878.
[6] H. Y. Kim, Y. J. Park, J. Kim, C. J. Han, J. Lee, Y. Kim, T. Greco, C. Ippen, A. Wedel, B.-K. Ju, M. S. Oh, *Adv. Funct. Mater.* **2016**, *26*, 3454.
[7] B. K. Hughes, J. M. Luther, M. C. Beard, *ACS Nano* **2012**, *6*, 4573.
[8] H. Moon, C. Lee, W. Lee, J. Kim, H. Chae, *Adv. Mater.* **2019**, *31*, 1804294.
[9] K. Zheng, K. Karki, K. Žídek, T. Pullerits, *Nano Res.* **2015**, *8*, 2125.
[10] J. Lim, M. Park, W. K. Bae, D. Lee, S. Lee, C. Lee, K. Char, *ACS Nano* **2013**, *7*, 9019.
[11] J. Lim, W. K. Bae, D. Lee, M. K. Nam, J. Jung, C. Lee, K. Char, S. Lee, *Chem. Mater.* **2011**, *23*, 4459.
[12] G. H. Nath, M. Sourav, D. Jayanta, *Chem. - Eur. J.* **2018**, *25*, 692.
[13] P. Reiss, M. Protière, L. Li, *Small* **2009**, *5*, 154.
[14] H. Li, C. Jia, X. Meng, H. Li, *Front. Chem.* **2019**, *6*, 652.
[15] E. R. Smith, J. M. Luther, J. C. Johnson, *Nano Lett.* **2011**, *11*, 4923.
[16] N. Siemons, A. Serafini, *J. Nanotechnol.* **2018**, *2018*, 1.
[17] S. Kershaw, A. Rogach, *Materials* **2017**, *10*, 1095.
[18] F. C. M. Spoor, G. Grimaldi, C. Delerue, W. H. Evers, R. W. Crisp, P. Geiregat, Z. Hens, A. J. Houtepen, L. D. A. Siebbeles, *ACS Nano* **2018**, *12*, 4796.
[19] G. Grimaldi, R. W. Crisp, S. ten Brinck, F. Zapata, M. van Ouwendorp, N. Renaud, N. Kirkwood, W. H. Evers, S. Kinge, I. Infante, L. D. A. Siebbeles, A. J. Houtepen, *Nat. Commun.* **2018**, *9*, 2310.
[20] Y. Yan, R. W. Crisp, J. Gu, B. D. Chernomordik, G. F. Pach, A R. Marshall, J. A. Turner, M. C. Beard, *Nat. Energy* **2017**, *2*, 17052.
[21] R. D. Schaller, V. I. Klimov, *Phys. Rev. Lett.* **2004**, *92*, 186601.
[22] D. M. Kroupa, G. F. Pach, M. Vörös, F. Giberti, B. D. Chernomordik, R. W. Crisp, A. J. Nozik, J. C. Johnson, R. Singh, V. I. Klimov, G. Galli, M. C. Beard, *ACS Nano* **2018**, *12*, 10084.
[23] A. Piryatinski, S. A. Ivanov, S. Tretiak, V. I. Klimov, *Nano Lett.* **2007**, *7*, 108.
[24] C. M. Cirloganu, L. A. Padilha, Q. Lin, N. S. Makarov, K. A. Velizhanin, H. Luo, I. Robel, J. M. Pietryga, V. I. Klimov, *Nat. Commun.* **2014**, *5*, 4148.
[25] S. ten Cate, Y. Liu, C. Suchand Sandeep, S. Kinge, A. J. Houtepen, T. J. Savenije, J. M. Schins, M. Law, L. D. Siebbeles, *J. Phys. Chem. Lett.* **2013**, *4*, 1766.
[26] Y. Liu, J. Tolentino, M. Gibbs, R. Ihly, C. L. Perkins, Y. Liu, N. Crawford, J. C. Hemminger, M. Law, *Nano Lett.* **2013**, *13*, 1578.
[27] A. Pourret, P. Guyot-Sionnest, J. W. Elam, *Adv. Mater.* **2009**, *21*, 232.
[28] *Atomic Layer Deposition in Energy Conversion Applications* (Ed: J. Bachmann), Wiley-VCH, Weinheim, Germany **2017**.
[29] M. K. S. Barr, L. Assaud, Y. Wu, C. Laffon, P. Parent, J. Bachmann, L. Santinacci, *Electrochim. Acta* **2015**, *179*, 504.
[30] M. Kulmas, L. Paterson, K. Höflich, M. Y. Bashouti, Y. Wu, M. Göbelt, J. Ristein, J. Bachmann, B. Meyer, S. Christiansen, *Adv. Funct. Mater.* **2016**, *26*, 4882.
[31] M. Ylilammi, O. M. E. Ylivaara, R. L. Puurunen, *J. Appl. Phys.* **2018**, *123*, 205301.
[32] W. Szmyt, C. Guerra, I. Utke, *Beilstein J. Nanotechnol.* **2017**, *8*, 64.
[33] J. Kuhs, A. Werbrouck, N. Zawacka, E. Drijvers, P. F. Smet, Z. Hens, C. Detavernier, *ACS Appl. Mater. Interfaces* **2019**, *11*, 26277.
[34] R. Beetstra, U. Lafont, J. Nijenhuis, E. M. Kelder, J. R. van Ommen, *Chem. Vap. Deposition* **2009**, *15*, 227.
[35] S. M. George, *Chem. Rev.* **2010**, *110*, 111.
[36] H. Van Bui, F. Grillo, J. R. van Ommen, *Chem. Commun.* **2017**, *53*, 45.
[37] R. L. Z. Hoye, B. Ehrler, M. L. Böhm, D. Muñoz-Rojas, R. M. Altamimi, A. Y. Alyamani, Y. Vaynzof, A. Sadhanala, G. Ercolano, N. C. Greenham, R. H. Friend, J. L. MacManus-Driscoll, K. P. Musselman, *Adv. Energy Mater.* **2014**, *4*, 1301544.
[38] K. Lambert, J. Dendooven, C. Detavernier, Z. Hens, *Chem. Mater.* **2011**, *23*, 126.
[39] D. Valdesueiro, M. K. Prabhu, C. Guerra-Nunez, C. S. S. Sandeep, S. Kinge, L. D. A. Siebbeles, L. C. P. M. de Smet, G. M. H. Meesters, M. T. Kreutzer, A. J. Houtepen, J. R. van Ommen, *J. Phys. Chem. C* **2016**, *120*, 4266.

[40] R. Ihly, J. Tolentino, Y. Liu, M. Gibbs, M. Law, *ACS Nano* **2011**, *5*, 8175.
[41] Y. Liu, M. Gibbs, C. L. Perkins, J. Tolentino, M. H. Zarghami, J. Bustamante, M. Law, *Nano Lett.* **2011**, *11*, 5349.
[42] O. G. Reid, D. T. Moore, Z. Li, D. Zhao, Y. Yan, K. Zhu, G. Rumbles, *J. Phys. D: Appl. Phys.* **2017**, *50*, 493002.
[43] O. G. Reid, M. Yang, N. Kopidakis, K. Zhu, G. Rumbles, *ACS Energy Lett.* **2016**, *1*, 561.
[44] R. W. Crisp, R. Callahan, O. G. Reid, D. S. Dolzhnikov, D. V. Talapin, G. Rumbles, J. M. Luther, N. Kopidakis, *J. Phys. Chem. Lett.* **2015**, *6*, 4815.
[45] M. Aerts, C. S. Suchand Sandeep, Y. Gao, T. J. Savenije, J. M. Schins, A. J. Houtepen, S. Kinge, L. D. A. Siebbeles, *Nano Lett.* **2011**, *11*, 4485.
[46] J. E. Kroeze, T. J. Savenije, M. J. W. Vermeulen, J. M. Warman, *J. Phys. Chem. B* **2003**, *107*, 7696.
[47] Y. Gao, C. S. S. Sandeep, J. M. Schins, A. J. Houtepen, L. D. A. Siebbeles, *Nat. Commun.* **2013**, *4*, 2329.
[48] D. Friedrich, M. Kunst, *J. Phys. Chem. C* **2011**, *115*, 16657.
[49] J. S. Jur, G. N. Parsons, *ACS Appl. Mater. Interfaces* **2011**, *3*, 299.
[50] T. Tommi, K. Maarit, *Semicond. Sci. Technol.* **2014**, *29*, 043001.
[51] V. Srikant, D. R. Clarke, *J. Appl. Phys.* **1998**, *83*, 5447.
[52] C. Weigand, R. Crisp, C. Ladam, T. Furtak, R. Collins, J. Grepstad, H. Weman, *Thin Solid Films* **2013**, *545*, 124.
[53] J. M. Schins, E. Talgorn, *Rev. Sci. Instrum.* **2011**, *82*, 064703.
[54] M. S. Prévot, X. A. Jeanbourquin, W. S. Bourée, F. Abdi, D. Friedrich, R. van de Krol, N. Guijarro, F. Le Formal, K. Sivula, *Chem. Mater.* **2017**, *29*, 4952.
[55] G. Dicker, M. P. de Haas, L. D. A. Siebbeles, *Phys. Rev. B* **2005**, *71*, 155204.
[56] G. Dicker, M. P. de Haas, L. D. A. Siebbeles, J. M. Warman, *Phys. Rev. B* **2004**, *70*, 045203.
[57] G. D. Scholes, G. Rumbles, *Nat. Mater.* **2006**, *5*, 683.
[58] T. Kirchartz, B. E. Pieters, K. Taretto, U. Rau, *Phys. Rev. B* **2009**, *80*, 035334.
[59] L. M. Andersson, C. Müller, B. H. Badada, F. Zhang, U. Würfel, O. Inganäs, *J. Appl. Phys.* **2011**, *110*, 024509.
[60] E. A. Schiff, *Sol. Energy Mater. Sol. Cells* **2003**, *78*, 567.
[61] F. Grillo, D. La Zara, P. Mulder, M. T. Kreutzer, J. Ruud van Ommen, *J. Phys. Chem. C* **2018**, *122*, 19981.
[62] J. G. Berryman, *Phys. Rev. A* **1983**, *27*, 1053.
[63] W. M. Haynes, *CRC Handbook of Chemistry and Physics*, CRC Press, Boca Raton, Lodon, New York **2014**.
[64] E. Marino, D. M. Balazs, R. W. Crisp, D. Hermida-Merino, M. A. Loi, T. E. Kodger, P. Schall, *J. Phys. Chem. C* **2019**, *123*, 13451.
[65] E. Marino, T. E. Kodger, R. W. Crisp, D. Timmerman, K. E. MacArthur, M. Heggen, P. Schall, *Angew. Chem.* **2017**, *129*, 13983.
[66] E. M. Sanehira, A. R. Marshall, J. A. Christians, S. P. Harvey, P. N. Ciesielski, L. M. Wheeler, P. Schulz, L. Y. Lin, M. C. Beard, J. M. Luther, *Sci. Adv.* **2017**, *3*, eaao4204.
[67] R. W. Crisp, D. M. Kroupa, A. R. Marshall, E. M. Miller, J. Zhang, M. C. Beard, J. M. Luther, *Sci. Rep.* **2015**, *5*, 9945.
[68] S. Shao, J. Liu, H.-H. Fang, L. Qiu, G. H. ten Brink, J. C. Hummelen, L. J. A. Koster, M. A. Loi, *Adv. Energy Mater.* **2017**, *7*, 1701305.
[69] R. W. Crisp, N. Kirkwood, G. Grimaldi, S. Kinge, L. D. A. Siebbeles, A. J. Houtepen, *ACS Appl. Energy Mater.* **2018**, *1*, 6569.
[70] F. Pietra, N. Kirkwood, L. De Trizio, A. W. Hoekstra, L. Kleibergen, N. Renaud, R. Koole, P. Baesjou, L. Manna, A. J. Houtepen, *Chem. Mater.* **2017**, *29*, 5192.
[71] A. Nag, M. V. Kovalenko, J.-S. Lee, W. Liu, B. Spokoyny, D. V. Talapin, *J. Am. Chem. Soc.* **2011**, *133*, 10612.
[72] A. Goulas, J. Ruud van Ommen, *J. Mater. Chem. A* **2013**, *1*, 4647.
[73] R. W. Crisp, G. F. Pach, J. M. Kurley, R. M. France, M. O. Reese, S. U. Nanayakkara, B. A. MacLeod, D. V. Talapin, M. C. Beard, J. M. Luther, *Nano Lett.* **2017**, *17*, 1020.
[74] J. Zhang, B. D. Chernomordik, R. W. Crisp, D. M. Kroupa, J. M. Luther, E. M. Miller, J. Gao, M. C. Beard, *ACS Nano* **2015**, *9*, 7151.
[75] J. M. Kurley, M. G. Panthani, R. W. Crisp, S. U. Nanayakkara, G. F. Pach, M. O. Reese, M. H. Hudson, D. S. Dolzhnikov, V. Tanygin, J. M. Luther, D. V. Talapin, *ACS Energy Lett.* **2017**, *2*, 270.
[76] M. G. Panthani, J. M. Kurley, R. W. Crisp, T. C. Dietz, T. Ezzyat, J. M. Luther, D. V. Talapin, *Nano Lett.* **2014**, *14*, 670.
[77] R. W. Crisp, M. G. Panthani, W. L. Rance, J. N. Duenow, P. A. Parilla, R. Callahan, M. S. Dabney, J. J. Berry, D. V. Talapin, J. M. Luther, *ACS Nano* **2014**, *8*, 9063.